



1 Heterogeneous formation and light absorption of secondary organic
2 aerosols from acetone photooxidation: Remarkably enhancing effects
3 of seeds and ammonia

4
5
6 Si Zhang¹, Xinbei Xu¹, Luyao Chen¹, Can Wu^{1,2}, Zheng Li¹, Rongjie Li¹, Binyu Xiao¹,
7 Xiaodi Liu¹, Rui Li^{1,2}, Fan Zhang^{1,2}, Gehui Wang^{1,2*}

8
9
10 ¹Key Lab of Geographic Information Science of the Ministry of Education, School of
11 Geographic Sciences, East China Normal University, Shanghai 200241, China

12 ²Institute of Eco-Chongming, 20 Cuinia Rd., Chongming, Shanghai 202150, China

13
14
15
16
17 *Corresponding author: Prof. Gehui Wang, Email: ghwang@geo.ecnu.edu.cn

18 Tel: 86-21-54341193, Fax: 86-21-54341122

19



20 **Abstract:** Secondary organic aerosols (SOA) from highly volatile organic compounds
21 (VOCs) are currently not well represented in numerical models as their heterogeneous
22 formation mechanisms in the atmosphere remain unclear. Based on the smog chamber
23 experiments, here we investigated the yield and formation pathway of SOA from acetone
24 photooxidation in the presence of preexisting haze particles ((NH₄)₂SO₄, and NH₄HSO₄) and
25 mineral dusts (Na₂SO₄) under ammonia-rich conditions. Our results showed that the yield of
26 acetone-derived SOA can be remarkably enhanced via multiphase reactions in the presence
27 of these preexisting seeds especially for the mineral dusts, suggesting that heterogeneous
28 reactions of highly volatile VOCs is an important source of atmospheric SOA. We found that
29 aerosol acidity is a key factor controlling the formation pathways of SOA, in which
30 carbonyls produced from acetone photooxidation dissolve into the aqueous phase of the
31 preexisting seeds and oligomerize into SOA that consist of larger molecules on the acidic
32 aerosols but smaller molecules on the neutral mineral aerosols. Moreover, light absorption
33 ability of SOA formed on (NH₄)₂SO₄ aerosols is stronger than that formed on Na₂SO₄
34 mineral particles especially in the presence of ammonia. Based on the yields obtained, we
35 estimated the importance of acetone-derived SOA in the global atmosphere, which is 9.5-
36 18.4 Tg yr⁻¹, equivalent to 8.5-16.4% of the global SOA budget, suggesting that
37 heterogeneous formation of highly volatile VOCs such as acetone is an importance source of
38 SOA in the atmosphere and should be accounted for in the future model studies.

39 **Keywords:** Volatile organic compounds; Photochemical oxidation; Aqueous-phase reaction;
40 Polymerization; Aerosol acidity.

41



42 **1. Introduction**

43 Secondary organic aerosols (SOA) are the major component of fine particles in the
44 atmosphere and produced from the photochemical oxidation of volatile organic compounds
45 (VOCs) (Zhang et al., 2015a; Srivastava et al., 2022; Wang et al., 2016b), which
46 significantly affects human health and global climate change (Jo et al., 2023; Chowdhury et
47 al., 2022). However, current numeric models cannot predict the evolution of atmospheric
48 SOA accurately; one of reasons is that models often only consider the partitioning process of
49 condensable oxidation products of VOCs as the major formation pathway of SOA and
50 neglect the contribution of heterogeneous reactions of highly volatile VOCs to atmospheric
51 SOA (Heald et al., 2005; Li et al., 2023).

52 A number of researchers have reported that SOA formation can be promoted
53 significantly in the presence of hydrated seeds by heterogeneous reactions (Wong et al.,
54 2015; Nguyen et al., 2014; Liu et al., 2018; Ge et al., 2017). For instance, Wong et al. (2015)
55 reported that more isoprene SOA was formed on deliquescent ammonium sulfate seeds in
56 comparison with that on the efflorescent ones. Such an enhancing effect of multiphase
57 chemistry on SOA formation has also be found by Liu et al. (2018) and Wang et al. (2022) in
58 their laboratory experiments. Their results showed that SOA multiphase formation is
59 affected by the aerosol liquid phase properties such as acidity, ionic strength and mixing
60 state, which can alter the gas-to-particle phase partitioning of VOC and change the
61 formation process of SOA (Zhang et al., 2023; Riva et al., 2019; Riva et al., 2016; Bateman
62 et al., 2014; Kampf et al., 2013; Wei et al., 2022). Amorim et al. (2020) analyzed the OH
63 reactivities of formic acid in aqueous phases with different pH, and found that all the OAs
64 exhibited larger OH reactivities under basic conditions than those under acidic conditions,
65 indicating that aerosol acidity can influence the gas-particle partitioning and the
66 multigeneration oxidation of highly volatile organics in liquid phase (Wei et al., 2022;
67 Amorim et al., 2021; Amorim et al., 2020; Zhao et al., 2006; Lv et al., 2022). Moreover, a
68 few studies reported that the uptake of VOC oxidation products by inorganic aerosols is of
69 salting-in/salting-out effects (Waxman et al., 2015; Wang et al., 2016a). These results
70 suggest that heterogeneous reactions of highly volatile VOCs are probably important sources



71 of atmospheric SOA, although they are not currently included in chemical transport models
72 (Heald et al., 2005; Li et al., 2023).

73 Acetone is one of the highly volatile VOCs with a saturated vapor of more than 10 kPa
74 at 20°C, and abundantly exists in the atmosphere from the ground surface to the upper
75 troposphere (Seinfeld and Pandis, 2006). Acetone can be directly emitted from the natural
76 and anthropogenic sources and indirectly produced from oxidation of hydrocarbons (Jacob
77 et al., 2002; Wang et al., 2023). A laboratory experiment showed that deliquesced inorganic
78 aerosols may promote SOA formation from the photochemical oxidation of acetone (Ge et
79 al., 2017), but up to now the yield of SOA derived from acetone oxidation and the impact of
80 inorganic aerosol physicochemical properties on SOA formation from acetone have not been
81 reported. Therefore, the formation mechanism and the importance of acetone-derived SOA
82 in the real atmosphere remain unclear, where acetone ubiquitously co-exists with NH₃ and
83 preexisting aerosols.

84 In this work, we quantitatively investigated the effects of deliquescent seeds and NH₃
85 on SOA formation from the photochemical oxidation of acetone via chamber experiments,
86 and compared the difference of SOA formation processes in the presence of different seed
87 particles. We for the first time revealed a key role of seed acidity in controlling the yield and
88 formation pathways of SOA from acetone photooxidation, in which NH₃ and dust particles
89 can greatly enhance the production and light absorption of acetone-derived SOA, resulting
90 in a large contribution to the global SOA loading.

91 **2. Experiments section**

92 **2.1 Materials and methods**

93 All batch mode experiments in this study were performed in a 4 m³ sealed Teflon smog
94 chamber (Figure S1). Firstly, zero air and seed particles were introduced into the chamber.
95 Then, acetone, H₂O₂ and NH₃ were introduced sequentially for the heterogeneous reactions.
96 The experiment details are reported by our previous studies (Ge et al., 2019; Zhang et al.,
97 2021; Liu et al., 2021a).

98 Briefly, zero air produced by the Zero Air Supply (Model 111 and Model 1150, Thermo
99 Scientific, USA) was used as the background gas in this study. Saturated water vapor flow



100 produced by bubbling zero air through ultrapure water (Milli Q, 18.2 M Ω , Millipore Ltd.,
101 USA) was introduced into the chamber for adjusting the relative humidity ($85\pm 1.0\%$ RH).
102 Three types of water-solutions containing Na₂SO₄, (NH₄)₂SO₄ and NH₄HSO₄ were nebulized
103 to produce seed particles. A polydisperse mode of wetted inorganic aerosols was generated
104 from the solutions by using a single jet atomizer (7388SJA, TSI) and directly introduced into
105 the chamber as droplets without any desiccation. Reactant gases including acetone, H₂O₂,
106 NH₃ and SO₂ were added separately into the chamber along with a N₂ flow using a glass
107 syringe (Liu et al., 2022; Liu et al., 2021b).

108 **2.2 Smog chamber experiments and characterization**

109 **2.2.1. Smog chamber experiments**

110 In this study, the chamber experiments can be divided into two phases: Phase I, SOA
111 formation from the photochemical oxidation of acetone by OH radicals on aerosols was
112 investigated, in which the OH radicals were produced from the photolysis of H₂O₂ under
113 254 nm UV irradiating conditions; Phase II, the effect of NH₃ on SOA formation was
114 explored under dark conditions. The influence of different inorganic particles on the two
115 phases were studied. To compare the influence of different inorganic particles on the SOA
116 formation, SO₂ was added into the chamber after Phase II to produce (NH₄)₂SO₄ aerosols
117 during the Na₂SO₄ seed experiments. All the experiments were conducted under $85\pm 1.0\%$
118 RH conditions and thus all the seeds in the chamber were deliquescent. At the end of each
119 experiment, aerosol in the chamber were collected on 47 mm quartz filters and stored at
120 $-20\text{ }^{\circ}\text{C}$ prior to analysis. The initial experimental conditions were displayed in Table S1.

121 **2.2.2. On-line monitoring**

122 RH and temperature inside the chamber were monitored online. The temperature in the
123 chamber was stabilized at $25\pm 1^{\circ}\text{C}$ by using air conditioners. Concentrations of VOCs and
124 SO₂ in the chamber were monitored by a proton transfer reaction time-of-flight mass
125 spectrometer (PTR-TOF-MS, Ionicon Analytik, Innsbruck, Austria) and a SO₂ analyzer
126 (Model 43i, Thermo scientific), respectively. Size distribution and mass concentration of
127 aerosols during the reaction process were measured by a scanning mobility particle sizer
128 (SMPS, model 3082, USA). The real-time chemical composition evolution of aerosols in the



129 chamber was measured by a high-resolution time-of-flight aerosol mass spectrometer (HR-
130 ToF-AMS, Aerodyne Research Ltd, USA), which was operated on a high sensitivity V-mode
131 with a 30 s time resolution. Prior to the experiments, ionization efficiency of the AMS was
132 calibrated by using 300 nm NH_4NO_3 particles and the value was 5.01×10^{-8} , and the relative
133 ionization efficiency (RIE) for ammonium was 4.6. The RIE for sulfate was calibrated using
134 $(\text{NH}_4)_2\text{SO}_4$ particles, and the value was 0.8.

135 Particle wall loss in the chamber was corrected using a total-mass-concentration-based
136 method and the detailed descriptions were shown in Text S1 (Liu and Abbatt, 2021; Zhang et
137 al., 2024). The wall loss of NH_3 and VOCs in the chamber was also corrected (see the details
138 in Text S2 and S3) (Li et al., 2021a; Huang et al., 2018; Zhang et al., 2015b). Aerosol liquid
139 water content (ALWC) was estimated using the E-AIM thermodynamic model IV, and the
140 pH values of aerosols were calculated by Eq.1.

$$\text{pH} = -\log_{10} (\gamma_{\text{H}^+} m_{\text{H}^+}) \quad (1)$$

141 Where γ_{H^+} and m_{H^+} were the activity coefficient and molality of H^+ , respectively.

142 **2.2.3. Off-line analysis of particles**

143 The collected samples were extracted with 15 mL of Milli-Q pure water in an ultrasonic
144 bath for 30 min, and filtered by a 0.45 μm PES syringe filter. The concentration of water-
145 soluble organic carbon (WSOC) and light absorption of the extracts were analyzed by a total
146 organic carbon analyzer (model TOC/TN-LCPH, Shimadzu Inc. Japan) and a liquid
147 waveguide capillary cell (model LWCC3000, Ocean Insight. USA) coupled with a UV/Vis
148 spectrophotometer (ocean insight) over a wavelength range of 200–900 nm, respectively.
149 Light absorption (Abs_λ) and mass absorption coefficient (MAC) of the water extracts were
150 calculated (see the details in Text S5). In addition, the collected particles were extracted with
151 pure methanol and analyzed for their chemical compositions using an ultrahigh-resolution
152 orbitrap mass spectrometer (Q-Exactive Orbitrap mass spectrometer, Thermo Scientific,
153 Germany) (Jia et al., 2023). Specifically, imidazole compounds (IMs) were determined using
154 the orbitrap-mass spectrometry, and the detailed analysis methods were reported in our
155 previous study (Liu et al., 2023).

156 **3. Results and discussion**



157 **3.1. Formation of acetone-derived SOA**

158 Figure 1 shows the time evolution of gas and particle phase species during the reaction
159 in the presence of $(\text{NH}_4)_2\text{SO}_4$ seeds. In this study the whole smog chamber reaction process
160 consists of two phases, of which Phase I is a photooxidation of acetone by OH radicals
161 without $\text{NH}_3(\text{g})$ and Phase II is a dark reaction with introduced NH_3 . During the Phase I,
162 once the light was turned on the gas phase concentrations of MGly, acetaldehyde, formic
163 acid and acetic acid quickly increased with a decreasing acetone (Phase I, Figure 1a), while
164 SOA were instantly produced and sharply increased to over $90 \mu\text{g m}^{-3}$ (Phase I, Figure 1b).
165 When the concentration of SOA during the Phase I did not change and even started to
166 decrease, the light was turned off and $\text{NH}_3(\text{g})$ was introduced into the chamber (Phase II).
167 According to the formation time of these gas products, acetaldehyde and MGly are often
168 taken as the first-generation products, while formic and acetic acids are usually considered
169 as the final-generation products (Poulain et al., 2010). Oxidation state of compounds (OSc)
170 and O/C elemental ratio of SOA in the aerosol phase continuously increased during the
171 reaction process (Figure 1c), which is corresponding to a decreasing fraction of CHO^+ plus
172 $\text{C}_2\text{H}_3\text{O}^+$ and an increasing fraction of CO_2^+ (Figure 1d), indicating an efficient conversion of
173 carbonyl compounds to carboxylic acid compounds. In the Phase I, we observed an aerosol-
174 phase decreasing trend of molar ratio of NH_4^+ to SO_4^{2-} , which was accompanied by an
175 increasing trend of N/C ratio of SOA (Figures 1b and 1c), indicating a transformation of
176 inorganic NH_4^+ to N-containing organic compounds. Such a phenomenon can be ascribed to
177 a reaction of carbonyl compounds with the $(\text{NH}_4)_2\text{SO}_4$ seeds during the Phase I (Liu et al.,
178 2023; Li et al., 2021b).

179 As shown in Figures 1a and 1b, after NH_3 was introduced (Phase II) the formic and
180 acetic acids decreased dramatically while SOA did not change obviously, suggesting that the
181 decreases of the gas acids were mainly resulted from the enhanced wall loss due to the
182 neutralization of NH_3 on the chamber wall. Interestingly, we found that during the dark
183 reaction OSc and O/C ratio of SOA decreased slightly but their N/C ratio increased
184 significantly by a factor of approximately two (Figure 1c), implying that chemical
185 composition of SOA changed remarkably after NH_3 was introduced, although the SOA mass



186 did not change evidently (Figure 1c, Phase II). Moreover, such a slight decrement of O/C
187 and a significant increment of N/C in the elemental compositions of SOA (Figure 1c) were
188 also accompanied by a sharp increase of CHN family fragment fractions (Figure 1d, Phase
189 II), which can be explained by a carbonyl-ammonium condensation under the dark
190 conditions that forms a C-N bond and loses a H₂O molecule (Aiona et al., 2017; Li et al.,
191 2021b; Liu et al., 2023). Such an aqueous-phase dark reaction after NH₃ was introduced can
192 be further revealed by a change in SOA composition during the Phase II, which is
193 characterized by higher fractions of C_xH_yN₁ fragments in the Phase II than those in the
194 Phase I (Figure 2). Organic ammonium salt would contribute NH_x fragments instead of
195 fragments containing N, C, and O elements. Therefore, the CHN species should generated
196 from the reactions of carbonyls with NH₃ rather than the acid-base neutralization of organic
197 acid with NH₃ (Liu et al., 2015). As seen in Figure S2, the CHN family species mainly
198 include CHN, CH₄N, C₂H₆N, C₂H₇N, C₂H₄N, CH₅N and C₃H₆N ions, which are similar to
199 the fragments of N-containing organics produced from the reaction of carbonyls with
200 (NH₄)₂SO₄ (De Haan et al., 2010), and increased significantly during the Phase II, resulting
201 in an enhancing role of NH₃ on the SOA formation from acetone photochemical oxidation.

202 **3.2. Enhancing effect of seeds on the SOA formation**

203 As shown in Figure S3, the concentration of SOA derived from acetone photooxidation
204 in the presence of (NH₄)₂SO₄ seeds is twenty times higher than that in the absence of the
205 seeds, suggesting that the occurrence of (NH₄)₂SO₄ seeds remarkably promoted the SOA
206 formation. Such an enhancing role was also found for Na₂SO₄ and NH₄HSO₄ seeds (Figure
207 S4). Because of the significant influence of surface area of aerosols on the multiphase
208 reactions (Huang et al., 2016), the SOA formation amounts were normalized by the aerosol
209 surface area (SA) to eliminate the interference of the difference in seed concentrations. As
210 seen in Figure 3a, the normalized concentration of SOA on Na₂SO₄ seeds is two times larger
211 than that on (NH₄)₂SO₄ and NH₄HSO₄ seeds, respectively, indicating that the difference in
212 physicochemical properties of seeds are of different promoting effects on the SOA
213 formation. MGly is one of the first-generation oxidation products of the acetone-OH
214 reaction and also the critical precursor of SOA (Li et al., 2021b). Therefore, we choose it as



215 the target compound to explore the effect of the seeds on the SOA formation. The
216 multiphase reactions of acetone-derived MGly in the chamber can be divided into two
217 processes: the gas-particle partitioning and the subsequent aqueous phase reactions
218 (Srivastava et al., 2022; Waxman et al., 2015), which are further discussed as follows:

219 **3.2.1. The effects on the gas-to-particle phase partitioning**

220 It has been reported that the presence of salts in aerosol aqueous phase can significantly
221 influence the gas-particle phase partitioning of MGly, which can decrease the solubility of
222 MGly, i.e., salting out effect (Waxman et al., 2015). In this study, the effective Henry's law
223 constants ($K_{H, \text{salt}}$) of MGly in the aqueous phase of various seeds were further estimated by
224 Eq.2 (Waxman et al., 2015; Cui et al., 2021).

$$\log \left(\frac{K_{H,w}}{K_{H,salt}} \right) = K_S c_{salt} \quad (2)$$

225 Where $K_{H,w}$ and $K_{H, \text{salt}}$ are the Henry's law constants of MGly in pure water ($3.71 \times 10^3 \text{ M}$
226 atm^{-1}) (Curry et al., 2018) and in a salt solution, respectively; K_S is the salting constant or
227 Setschenow constant, which is 0.16 M^{-1} used in this work (Waxman et al., 2015), supposing
228 that the K_S values are similar in the three types of inorganic aerosols (Gen et al., 2018); c_{salt}
229 is the salt concentration in molality.

230 As shown in Figure 3b, $K_{H, \text{salt}}$ of MGly on Na_2SO_4 seeds in this study is more than two
231 times that on $(\text{NH}_4)_2\text{SO}_4$ and NH_4HSO_4 seeds, respectively, because of its lower salt
232 concentration and weaker salting out effect. The acidity of aerosol aqueous phase also can
233 affect the uptake of MGly. For instance, Zhao et al. (2006) found that the effective Henry's
234 law constant of MGly decreased with an increase of aqueous acidity in their laboratory
235 experiments. As shown in Figure 3b, the pH values of Na_2SO_4 , $(\text{NH}_4)_2\text{SO}_4$ and NH_4HSO_4
236 seeds in our chamber study are 7.0, 4.9 and -0.2, respectively, indicating that the neutral
237 nature of Na_2SO_4 seeds is more favorable for the uptake of MGly compared to the two other
238 acidic seeds. In addition, the higher OSc and larger fraction of $\text{C}_x\text{H}_y\text{O}_z$ signals of SOA on
239 Na_2SO_4 seeds (Figure 3a and Figure S5) may also be caused by enhanced uptake of
240 carboxylic acids (e.g., formic and acetic acids) in comparison with those by other two kinds
241 of acidic seeds (Huang et al., 2016).



242 **3.2.2. The effects on the aqueous reaction**

243 The aqueous formation of SOA could be affected by the phase state and acidity of
244 aerosols (Amorim et al., 2020; Amorim et al., 2021; Shen et al., 2022). Since particles in all
245 the experiments of this work are deliquesced under 85% RH conditions (Wong et al., 2015;
246 Bateman et al., 2015), the influence of phase state can be neglected. Here, we focus on the
247 impact of aerosol acidity on the SOA formation pathway by characterizing the chemical
248 composition of SOA in the chamber using ESI-Q-MS technique. The mass spectra of SOA
249 formed on different seeds are shown in Figures 3c and 3d, and the detail peak assignments
250 are presented in Table S2, respectively. As shown by Figures 3c and 3d, the main peaks of
251 SOA formed on Na₂SO₄ seeds locate in the mass range lower than $m/z=200$, whereas the
252 main peaks of SOA formed on (NH₄)₂SO₄ seeds locate in the mass range larger than
253 $m/z=200$, clearly showing that SOA formed on neutral aerosols are dominated smaller
254 molecules while those formed on acidic aerosols are dominated larger molecules. Such
255 different formation pathways of SOA can be explained by the difference of reactive oxygen
256 species formed in the aqueous phase of the different aerosols. On neutral aerosols, organic
257 hydroperoxides produced from the reaction of peroxides radicals and HO₂ radicals
258 decompose and generate OH radicals through the cleavage of the weaker O-O bond (Wei et
259 al., 2022). Then, the OH radicals oxidize the oligomers to low molecular weight (LMW)
260 compounds (Zhao et al., 2017). In contrast, on acidic aerosols the acid-catalyzed thermal
261 decomposition of the organic hydroperoxides leads to the formation of alcohol and ketone as
262 the end products, which does not involve radical formation (Wei et al., 2022; Yaremenko et
263 al., 2016). Then, the carbonyls in the aqueous phase will undergo hydration, oligomerization
264 and acid-catalyzed aldol condensation to form high molecular weight (HMW) compounds
265 (Zhang et al., 2015a; Kenseth et al., 2023; Li et al., 2021b). Such an explanation can be
266 supported by the higher OSc of SOA formed on the neutral aerosols (Figure 3a). On the
267 other hand, the lower SOA mass formed on acidic aerosols can also in part be attributed to
268 the different reactivity of OH radical to carboxylic group; OH radical does not react with the
269 carboxyl group (COOH) rapidly through H-abstraction from an O-H bond, but OH radical is
270 more reactive to the carboxylate group (ROO⁻) by abstracting an electron, which can result



271 in a high SOA yield on neutral aerosols (Amorim et al., 2021; Herrmann et al., 2015).

272 **3.3 The different effect of NH₃ on SOA formation on different seeds**

273 As shown in Figure 4a, when NH₃ was introduced into the reaction system (Phase II),
274 the ratio of N/C of SOA increased significantly because of the reaction of NH₄⁺/NH₃ with
275 carbonyls on acidic (NH₄)₂SO₄ and NH₄HSO₄ seeds, but such an evident change was not
276 observed in the presence of NH₃ for neutral Na₂SO₄ seeds. One of the reasons is that NH₃
277 dissolve more readily on acidic aerosols. The gas-to-particle phase partition coefficients of
278 NH₃ ($\epsilon(\text{NH}_4^+)$) on different seeds were calculated (Text S6) (Guo et al., 2017; Lv et al.,
279 2023). As shown in Figure 4b, $\epsilon(\text{NH}_4^+)$ is zero and 1.0 for Na₂SO₄ and NH₄HSO₄ seeds,
280 respectively, suggesting that NH₃ was almost not absorbed by Na₂SO₄ seeds but efficiently
281 absorbed by NH₄HSO₄ seeds. Liu et al. (2015) analyzed the uptake of NH₃ onto SOA and
282 also found that the uptake coefficient positively correlated with particle acidity. Several
283 studies put forward that the reaction of NH₃ with carbonyl are likely acid-catalyzed (Zhang
284 et al., 2015a; Liu et al., 2015). However, such a conclusion was inconsistent with the
285 phenomenon observed by Yang et al. (2024); they found that the light absorption ability of
286 brown carbon produced from the aqueous reactions of α -dicarbonyls with ammonium or
287 amine increased exponentially with the increase of pH. To resolve such a disagreement. We
288 analyzed the chemical composition of SOA detected by HR-ToF-AMS at different reaction
289 phases. As shown in Figure S5a-d, no change was observed on Na₂SO₄ particles at Phase II
290 after NH₃ was introduced, but the fraction of the CHN family species increased dramatically
291 on (NH₄)₂SO₄ and NH₄HSO₄ particles at phase II. Hence, we supposed that NH₃ can
292 promote the formation of N-containing SOA on acidic aerosols significantly via reacting
293 with carbonyl compounds. To verify such an assumption, we performed additional
294 experiments by introducing 500 ppb SO₂ into the chamber in the presence of Na₂SO₄ seeds
295 after Phase II (Phase III, Figure S6). The addition of SO₂ resulted in (NH₄)₂SO₄ produced
296 immediately in the chamber (Phase III, Figure S6a), and then the fraction of CHN species
297 increased sharply (Phase III, Figure S6b). Such results again demonstrate the pivotal role of
298 acidic particles in the formation of N-containing SOA.

299 The optical properties of the acetone-derived SOA on different particles were measured



300 by LWCC. Compared with the light absorption spectra of SOA formed on Na_2SO_4 seeds in
301 the absence of SO_2 , an enhanced MAC peak at ~ 270 nm was observed for SOA formed on
302 $(\text{NH}_4)_2\text{SO}_4$ seeds and on Na_2SO_4 seeds with SO_2 , respectively (Figure 4c). Such enhanced
303 absorptions are in agreement with that of the products from MGly and $(\text{NH}_4)_2\text{SO}_4$ reaction,
304 which displays prominent peaks at <240 and ~ 270 nm with a tail extending to >350 nm
305 (Kasthuriarachchi et al., 2020). The increased absorption peak at 270 nm can be ascribed to
306 a formation of imidazoles through the reaction of MGly with NH_4^+ (You et al., 2020). In this
307 work, 1H-imidazole-4-carboxylic acid was observed for the SOA formed on $(\text{NH}_4)_2\text{SO}_4$
308 seeds (Figure 4d). However, there was no absorption peak at ~ 270 nm for the products of the
309 Na_2SO_4 particles in the absence of SO_2 (Figure 4c), further confirming the enhancement
310 effect of acidic particles on the formation of light-absorbing SOA, which is often termed as
311 brown carbon.

312 **3.4. Formation mechanisms of acetone-derived SOA on different seeds**

313 Figure 5 shows the mass yield and MAC of acetone-derived SOA at the end of Phase
314 II. Clearly, SOA is formed more readily on neutral Na_2SO_4 seeds than on acidic $(\text{NH}_4)_2\text{SO}_4$
315 seeds. However, in the presence of NH_3 , SOA formed on $(\text{NH}_4)_2\text{SO}_4$ seeds are more light-
316 absorbing than those formed on Na_2SO_4 aerosols, suggesting that a stronger acidity of
317 aerosol phase is favorable for the formation of light-absorbing organics, because NH_3 cannot
318 be taken up by neutral aerosols and thus carbonyl-ammonium condensation is only active
319 under acidic conditions and produce light-absorbing N-containing organics.

320 By combining the gas and aerosol phase chemistry evolution in the chamber, chemical
321 mechanism for SOA formation from acetone-OH multiphase oxidation on different aerosols
322 in the presence of NH_3 was proposed (Figure 6). The first-generation products in the
323 oxidation of acetone by OH radicals are carbonyls including MGly, acetaldehyde,
324 formaldehyde and acetone alcohol. One part of those gas-phase carbonyls are oxidized to
325 carboxylic acids such as formic and acetic acids and another part of those are absorbed by
326 the aerosol liquid phase and undergo a series of liquid phase reactions (Poulain et al., 2010).
327 For example, the dissolved MGly can be hydrolyzed and then oxidized to organic acids such
328 as pyruvic and oxalic acids or proceeds to a series of oligomerizations to produce many



329 oligomers, giving rise to SOA formation.

330 In the presence of NH_4^+ , carbonyl compounds in the aerosol phase can react with free
331 NH_3 molecules and produce N-containing SOA including imine, imidazole and other
332 oligomers (Liu et al., 2023). LMW SOA are formed readily in neutral aerosol phase, while
333 HMW SOA and N-containing brown carbon are formed favorably in acidic aerosol phase,
334 because the acidic condition is favorable for the uptake of NH_3 . The carbenium cations,
335 which are produced from protonation and dehydration of the hydration products of MGly
336 under acidic conditions, are the key intermediates for formation and propagation of
337 oligomerization (Ji et al., 2020). The oligomers and N-heterocycles are produced from the
338 nucleophilic addition of the negative hydroxyl O-atom of hydration products and the
339 negative N-atom of NH_3 to the carbenium cations, respectively (Li et al., 2021b; Li et al.,
340 2021a).

341 **3.5. Contribution of acetone-derived SOA to the global SOA**

342 Currently, estimations of acetone-derived SOA by models only consider its product
343 MGly as the precursor (Fu et al., 2008). The uptake coefficient (γ) of MGly is set as $2.6 \times$
344 10^{-4} in CMAQ v5.3 in general (Chen et al., 2021). Hence, the concentration of SOA formed
345 in the chamber only from the irreversible uptake of MGly can be calculated by Eq.3 (Chen
346 et al., 2021; Li et al., 2023).

$$\frac{\partial aqSOA}{\partial t} = \left(\frac{a}{D_g} + \frac{4}{v_{MGLY}\gamma_{MGLY}} \right)^{-1} A[MGLY] \quad (3)$$

347 Where $\frac{\partial aqSOA}{\partial t}$ is the formation rate of SOA in experiments; a is the effective radius of
348 aerosols; D_g is the gas-phase molecular diffusion coefficient; v_{MGLY} is the gas-phase mean
349 molecular speed of MGly; A is the aerosol surface area per unit air volume; $[MGLY]$ is the
350 vapor-wall loss corrected concentration of MGly (see the details in Text S3).

351 As shown in Table S3, the concentrations of the total SOA-derived from acetone
352 oxidation in the chamber is 2.83-8.15 times that only from the irreversible uptake of MGly,
353 indicating that only considering the role of MGly will inevitably underestimate the
354 contribution of acetone to SOA production in the atmosphere. Therefore, here we re-



355 calculate the loading of acetone-derived SOA in the global atmosphere based on the yields
356 obtained by this chamber study. The global budgets of acetone and SOA are about 95 and
357 112 Tg yr⁻¹, respectively (Li et al., 2021b; Jacob et al., 2002). (NH₄)₂SO₄ and NH₄HSO₄
358 aerosols are ubiquitous in the atmosphere, and the acetone-SOA mass yields measured by
359 this work are 10% and 19.4% in the presence of NH₄HSO₄ and (NH₄)₂SO₄ seeds,
360 respectively. Thus, we use these two yields to roughly estimate the acetone-derived SOA in
361 the global atmosphere, which is 9.5-18.4 Tg yr⁻¹, equivalent to 8.5-16.4% of the global SOA
362 budget, suggesting an importance of the contribution of SOA formed from the multiphase
363 oxidation of acetone in the atmosphere. The above simple estimation is of high uncertainty,
364 but our work provided a strong evidence that the heterogeneous oxidation of highly volatile
365 VOC, for example acetone, is an importance source of SOA in the atmosphere and should be
366 accounted for in the future model studies.

367 **4. Conclusions**

368 In this study we investigated the mass yield and formation mechanism of SOA from
369 acetone photooxidation in the presence of preexisting haze particles ((NH₄)₂SO₄ and
370 NH₄HSO₄) and mineral dusts (Na₂SO₄) under ammonia-rich conditions. We found that the
371 presence of seeds can significantly promote the formation of acetone-derived SOA, and the
372 SOA yield on Na₂SO₄ seeds is larger than that on acidic (NH₄)₂SO₄ and NH₄HSO₄ seeds,
373 indicating that the differences in physicochemical properties of pre-existing aerosols are of
374 different promoting effects on the acetone-derived SOA formation. In comparison with those
375 of (NH₄)₂SO₄, and NH₄HSO₄ seeds, the weaker salting-out effect and lower acidity of
376 Na₂SO₄ seeds are in favor of the gas-to-particle partitioning of the SOA precursor. Moreover,
377 SOA formed on the neutral seeds are dominated by smaller molecules with a higher OSc,
378 while those formed on the acidic seeds are dominated by larger molecules with a lower OSc.

379 Because NH₃ cannot be taken up by neutral aerosols, heterogeneous reaction of
380 carbonyl with ammonium is only active under acidic conditions, which produces light-
381 absorbing N-containing compounds such as imidazoles, resulting in the SOA formed on
382 (NH₄)₂SO₄ seeds more light absorbing than those formed on Na₂SO₄ seeds. Our work
383 suggests that only considering the irreversible uptake of MGly will inevitably underestimate



384 the contribution of acetone photooxidation to SOA in the atmosphere, and also provides a
385 strong evidence that the heterogeneous oxidation of highly volatile VOC, for example
386 acetone, is an importance source of SOA in the atmosphere, which should be accounted for
387 in the future model studies.

388

389 **ASSOCIATED CONTENT**

390 **Supplement.** The supplement related to this article is available online at: <https://doi.org/XX>.

391 **Author contribution.** SZ and GW designed the experiment. SZ, XX, and LC conducted the
392 experiments. SZ, XX, LC, and GW performed the data interpretation. SZ and GW wrote the
393 paper. CW, RL, FZ, ZL, and RL contributed to the paper with useful scientific discussions
394 or comments.

395 **Competing interests.** The authors declare no competing financial interest.

396 **Disclaimer.**

397 **Acknowledgements.**

398 This work was funded by the National Natural Science Foundation of China (No.
399 42130704, U23A2030).

400 **References:**

- 401 Aiona, P. K., Lee, H. J., Leslie, R., Lin, P., Laskin, A., Laskin, J., and Nizkorodov, S. A.: Photochemistry of
402 products of the aqueous reaction of methylglyoxal with ammonium sulfate, *ACS Earth Space Chem.*, 1,
403 522-532, 10.1021/acsearthspacechem.7b00075, 2017.
- 404 Amorim, J. V., Guo, X., Gautam, T., Fang, R., Fotang, C., Williams, F. J., and Zhao, R.: Photo-oxidation of pinic
405 acid in the aqueous phase: a mechanistic investigation under acidic and basic pH conditions, *Environ. Sci.*
406 *Atmos.*, 1, 276-287, 10.1039/d1ea00031d, 2021.
- 407 Amorim, J. V., Wu, S., Klimchuk, K., Lau, C., Williams, F. J., Huang, Y., and Zhao, R.: pH dependence of the
408 OH reactivity of organic acids in the aqueous phase, *Environ. Sci. Technol.*, 54, 12484-12492,
409 10.1021/acs.est.0c03331, 2020.
- 410 Bateman, A. P., Bertram, A. K., and Martin, S. T.: Hygroscopic influence on the semisolid-to-liquid transition of
411 secondary organic materials, *J. Phys. Chem. A*, 119, 4386-4395, 10.1021/jp508521c, 2014.
- 412 Bateman, A. P., Gong, Z., Liu, P., Sato, B., Cirino, G., Zhang, Y., Artaxo, P., Bertram, A. K., Manzi, A. O., Rizzo,
413 L. V., Souza, R. A. F., Zaveri, R. A., and Martin, S. T.: Sub-micrometre particulate matter is primarily in
414 liquid form over Amazon rainforest, *Nature Geosci.*, 9, 34-37, 10.1038/ngeo2599, 2015.
- 415 Chen, X. Y., Zhang, Y., Zhao, J., Liu, Y. M., Shen, C., Wu, L. Q., Wang, X. M., Fan, Q., Zhou, S. Z., and Hang,
416 J.: Regional modeling of secondary organic aerosol formation over eastern China: The impact of uptake
417 coefficients of dicarbonyls and semivolatile process of primary organic aerosol, *Sci. Total Environ.*, 793,



- 148176, 10.1016/j.scitotenv.2021.148176, 2021.
- Chowdhury, S., Pozzer, A., Haines, A., Klingmüller, K., Münzel, T., Paasonen, P., Sharma, A., Venkataraman, C., and Lelieveld, J.: Global health burden of ambient PM_{2.5} and the contribution of anthropogenic black carbon and organic aerosols, *Environ. Int.*, 159, 107020, 10.1016/j.envint.2021.107020, 2022.
- Cui, J. n., Sun, M., Wang, L., Guo, J., Xie, G., Zhang, J., and Zhang, R.: Gas-particle partitioning of carbonyls and its influencing factors in the urban atmosphere of Zhengzhou, China, *Sci. Total Environ.*, 751, 142027, 10.1016/j.scitotenv.2020.142027, 2021.
- Curry, L. A., Tsui, W. G., and McNeill, V. F.: Technical note: Updated parameterization of the reactive uptake of glyoxal and methylglyoxal by atmospheric aerosols and cloud droplets, *Atmos. Chem. Phys.*, 18, 9823-9830, 10.5194/acp-18-9823-2018, 2018.
- De Haan, D. O., Hawkins, L. N., Kononenko, J. A., Turley, J. J., Corrigan, A. L., Tolbert, M. A., and Jimenez, J. L.: Formation of nitrogen-containing oligomers by methylglyoxal and amines in simulated evaporating cloud droplets, *Environ. Sci. Technol.*, 45, 984-991, 10.1021/es102933x, 2010.
- Fu, T. M., Jacob, D. J., Wittrock, F., Burrows, J. P., Vrekoussis, M., and Henze, D. K.: Global budgets of atmospheric glyoxal and methylglyoxal, and implications for formation of secondary organic aerosols, *J. Geophys. Res.: Atmos.*, 113, D15303, 10.1029/2007jd009505, 2008.
- Ge, S., Wang, G., Zhang, S., Li, D., Xie, Y., Wu, C., Yuan, Q., Chen, J., and Zhang, H.: Abundant NH₃ in China enhances atmospheric HONO production by promoting the heterogeneous reaction of SO₂ with NO₂, *Environ. Sci. Technol.*, 53, 14339-14347, 10.1021/acs.est.9b04196, 2019.
- Ge, S. S., Xu, Y. F., and Jia, L.: Effects of inorganic seeds on secondary organic aerosol formation from photochemical oxidation of acetone in a chamber, *Atmos. Environ.*, 170, 205-215, 10.1016/j.atmosenv.2017.09.036, 2017.
- Gen, M., Huang, D. D., and Chan, C. K.: Reactive Uptake of Glyoxal by Ammonium-Containing Salt Particles as a Function of Relative Humidity, *Environ. Sci. Technol.*, 52, 6903-6911, 10.1021/acs.est.8b00606, 2018.
- Guo, H., Liu, J., Froyd, K. D., Roberts, J. M., Veres, P. R., Hayes, P. L., Jimenez, J. L., Nenes, A., and Weber, R. J.: Fine particle pH and gas-particle phase partitioning of inorganic species in Pasadena, California, during the 2010 CalNex campaign, *Atmos. Chem. Phys.*, 17, 5703-5719, 10.5194/acp-17-5703-2017, 2017.
- Heald, C. L., Jacob, D. J., Park, R. J., Russell, L. M., Huebert, B. J., Seinfeld, J. H., Liao, H., and Weber, R. J.: A large organic aerosol source in the free troposphere missing from current models, *Geophys. Res. Lett.*, 32, L18809, 10.1029/2005gl023831, 2005.
- Herrmann, H., Schaefer, T., Tilgner, A., Styler, S. A., Weller, C., Teich, M., and Otto, T.: Tropospheric aqueous-phase chemistry: Kinetics, mechanisms, and its coupling to a changing gas phase, *Chem. Rev.*, 115, 4259-4334, 10.1021/cr500447k, 2015.
- Huang, D. D., Zhang, X., Dalleska, N. F., Lignell, H., Coggon, M. M., Chan, C. M., Flagan, R. C., Seinfeld, J. H., and Chan, C. K.: A note on the effects of inorganic seed aerosol on the oxidation state of secondary organic aerosol— α -Pinene ozonolysis, *J. Geophys. Res.: Atmos.*, 121, 12476-12483, 10.1002/2016jd025999, 2016.
- Huang, Y., Zhao, R., Charan, S. M., Kenseth, C. M., Zhang, X., and Seinfeld, J. H.: Unified theory of vapor-wall mass transport in Teflon-walled environmental chambers, *Environ. Sci. Technol.*, 52, 2134-2142, 10.1021/acs.est.7b05575, 2018.
- Jacob, D. J., Field, B. D., Jin, E. M., Bey, I., Li, Q., Logan, J. A., Yantosca, R. M., and Singh, H. B.: Atmospheric budget of acetone, *J. Geophys. Res.: Atmos.*, 107, ACH 5-1-ACH 5-17, 10.1029/2001jd000694, 2002.
- Ji, Y. M., Shi, Q. J., Li, Y. X., An, T. C., Zheng, J., Peng, J. F., Gao, Y. P., Chen, J. Y., Li, G. Y., Wang, Y., Zhang, F., Zhang, A. L., Zhao, J. Y., Molina, M. J., and Zhang, R. Y.: Carbenium ion-mediated oligomerization of



- 462 methylglyoxal for secondary organic aerosol formation, *Proc. Natl. Acad. Sci.*, 117, 13294-13299,
463 10.1073/pnas.1912235117, 2020.
- 464 Jia, L., Xu, Y., and Duan, M.: Explosive formation of secondary organic aerosol due to aerosol-fog interactions,
465 *Sci. Total Environ.*, 866, 10.1016/j.scitotenv.2022.161338, 2023.
- 466 Jo, D. S., Nault, B. A., Tilmes, S., Gettelman, A., McCluskey, C. S., Hodzic, A., Henze, D. K., Nawaz, M. O.,
467 Fung, K. M., and Jimenez, J. L.: Global health and climate effects of organic aerosols from different sources,
468 *Environ. Sci. Technol.*, 57, 13793-13807, 10.1021/acs.est.3c02823, 2023.
- 469 Kampf, C. J., Waxman, E. M., Slowik, J. G., Dommen, J., Pfaffenberger, L., Praplan, A. P., Prévôt, A. S. H.,
470 Baltensperger, U., Hoffmann, T., and Volkamer, R.: Effective Henry's Law partitioning and the salting
471 constant of glyoxal in aerosols containing sulfate, *Environ. Sci. Technol.*, 47, 4236-4244,
472 10.1021/es400083d, 2013.
- 473 Kasthuriarachchi, N. Y., Rivellini, L. H., Chen, X., Li, Y. J., and Lee, A. K. Y.: Effect of relative humidity on
474 secondary brown carbon formation in aqueous droplets, *Environ. Sci. Technol.*, 54, 13207-13216,
475 10.1021/acs.est.0c01239, 2020.
- 476 Kenseth, C. M., Hafeman, N. J., Rezgui, S. P., Chen, J., Huang, Y., Dalleska, N. F., Kjaergaard, H. G., Stoltz, B.
477 M., Seinfeld, J. H., and Wennberg, P. O.: Particle-phase accretion forms dimer esters in pinene secondary
478 organic aerosol, *Science*, 382, 787-792, 10.1126/science.adi0857, 2023.
- 479 Li, J., Zhang, H., Li, L., Ye, F., Wang, H., Guo, S., Zhang, N., Qin, M., and Hu, J.: Modeling secondary organic
480 aerosols in China: State of the art and perspectives, *Curr. Pollut. Rep.*, 9, 22-45, 10.1007/s40726-022-00246-
481 3, 2023.
- 482 Li, Y. X., Zhao, J. Y., Wang, Y., Seinfeld, J. H., and Zhang, R. Y.: Multigeneration production of secondary
483 organic aerosol from toluene photooxidation, *Environ. Sci. Technol.*, 55, 8592-8603,
484 10.1021/acs.est.1c02026, 2021a.
- 485 Li, Y. X., Ji, Y. M., Zhao, J. Y., Wang, Y., Shi, Q. J., Peng, J. F., Wang, Y. Y., Wang, C. Y., Zhang, F., Wang, Y.
486 X., Seinfeld, J. H., and Zhang, R. Y.: Unexpected oligomerization of small alpha-dicarbonyls for secondary
487 organic aerosol and brown carbon formation, *Environ. Sci. Technol.*, 55, 4430-4439,
488 10.1021/acs.est.0c08066, 2021b.
- 489 Liu, S., Wang, Y., Xu, X., and Wang, G.: Effects of NO₂ and RH on secondary organic aerosol formation and
490 light absorption from OH oxidation of o-xylene, *Chemosphere*, 308, 10.1016/j.chemosphere.2022.136541,
491 2022.
- 492 Liu, S., Huang, D., Wang, Y., Zhang, S., Liu, X., Wu, C., Du, W., and Wang, G.: Synergetic effects of NH₃ and
493 NO_x on the production and optical absorption of secondary organic aerosol formation from toluene
494 photooxidation, *Atmos. Chem. Phys.*, 21, 17759-17773, 10.5194/acp-21-17759-2021, 2021a.
- 495 Liu, S. J., Wang, Y. Q., Wang, G. H., Zhang, S., Li, D. P., Du, L., Wu, C., Du, W., and Ge, S. S.: Enhancing effect
496 of NO₂ on the formation of light-absorbing secondary organic aerosols from toluene photooxidation, *Sci.
497 Total Environ.*, 794, 148714, 10.1016/j.scitotenv.2021.148714, 2021b.
- 498 Liu, T. and Abbatt, J. P. D.: Oxidation of sulfur dioxide by nitrogen dioxide accelerated at the interface of
499 deliquesced aerosol particles, *Nat. Chem.*, 13, 1173-1177, 10.1038/s41557-021-00777-0, 2021.
- 500 Liu, T., Huang, D. D., Li, Z., Liu, Q., Chan, M., and Chan, C. K.: Comparison of secondary organic aerosol
501 formation from toluene on initially wet and dry ammonium sulfate particles at moderate relative humidity,
502 *Atmos. Chem. Phys.*, 18, 5677-5689, 10.5194/acp-18-5677-2018, 2018.
- 503 Liu, X., Wang, H., Wang, F., Lv, S., Wu, C., Zhao, Y., Zhang, S., Liu, S., Xu, X., Lei, Y., and Wang, G.: Secondary
504 formation of atmospheric brown carbon in China haze: Implication for an enhancing role of ammonia,
505 *Environ. Sci. Technol.*, 57, 11163-11172, 10.1021/acs.est.3c03948, 2023.



- 506 Liu, Y., Liggio, J., Staebler, R., and Li, S. M.: Reactive uptake of ammonia to secondary organic aerosols: kinetics
507 of organonitrogen formation, *Atmospheric Chemistry and Physics*, 15, 13569-13584, 10.5194/acp-15-
508 13569-2015, 2015.
- 509 Lv, S., Wu, C., Wang, F., Liu, X., Zhang, S., Chen, Y., Zhang, F., Yang, Y., Wang, H., Huang, C., Fu, Q., Duan,
510 Y., and Wang, G.: Nitrate-enhanced gas-to-particle-phase partitioning of water-soluble organic compounds
511 in Chinese urban atmosphere: Implications for secondary organic aerosol formation, *Environ. Sci. Technol.*
512 *Letts.*, 10, 14-20, 10.1021/acs.estlett.2c00894, 2023.
- 513 Lv, S., Wang, F., Wu, C., Chen, Y., Liu, S., Zhang, S., Li, D., Du, W., Zhang, F., Wang, H., Huang, C., Fu, Q.,
514 Duan, Y., and Wang, G.: Gas-to-aerosol phase partitioning of atmospheric water-soluble organic compounds
515 at a rural site in China: An enhancing effect of NH₃ on SOA formation, *Environ. Sci. Technol.*, 56, 3915-
516 3924, 10.1021/acs.est.1c06855, 2022.
- 517 Nguyen, T. B., Coggon, M. M., Bates, K. H., Zhang, X., Schwantes, R. H., Schilling, K. A., Loza, C. L., Flagan,
518 R. C., Wennberg, P. O., and Seinfeld, J. H.: Organic aerosol formation from the reactive uptake of isoprene
519 epoxydiols (IEPOX) onto non-acidified inorganic seeds, *Atmos. Chem. Phys.*, 14, 3497-3510, 10.5194/acp-
520 14-3497-2014, 2014.
- 521 Poulain, L., Katrib, Y., Isikli, E., Liu, Y., Wortham, H., Mirabel, P., Le Calve, S., and Monod, A.: In-cloud
522 multiphase behaviour of acetone in the troposphere: Gas uptake, Henry's law equilibrium and aqueous phase
523 photooxidation, *Chemosphere*, 81, 312-320, 10.1016/j.chemosphere.2010.07.032, 2010.
- 524 Riva, M., Bell, D. M., Hansen, A.-M. K., Drozd, G. T., Zhang, Z., Gold, A., Imre, D., Surratt, J. D., Glasius, M.,
525 and Zelenyuk, A.: Effect of organic coatings, humidity and aerosol acidity on multiphase chemistry of
526 isoprene epoxydiols, *Environ. Sci. Technol.*, 50, 5580-5588, 10.1021/acs.est.5b06050, 2016.
- 527 Riva, M., Chen, Y., Zhang, Y., Lei, Z., Olson, N. E., Boyer, H. C., Narayan, S., Yee, L. D., Green, H. S., Cui, T.,
528 Zhang, Z., Baumann, K., Fort, M., Edgerton, E., Budisulistiorini, S. H., Rose, C. A., Ribeiro, I. O., e Oliveira,
529 R. L., dos Santos, E. O., Machado, C. M. D., Szopa, S., Zhao, Y., Alves, E. G., de Sá, S. S., Hu, W., Knipping,
530 E. M., Shaw, S. L., Duvoisin Junior, S., de Souza, R. A. F., Palm, B. B., Jimenez, J.-L., Glasius, M.,
531 Goldstein, A. H., Pye, H. O. T., Gold, A., Turpin, B. J., Vizuete, W., Martin, S. T., Thornton, J. A., Dutcher,
532 C. S., Ault, A. P., and Surratt, J. D.: Increasing isoprene epoxydiol-to-inorganic sulfate aerosol ratio results
533 in extensive conversion of inorganic sulfate to organosulfur forms: Implications for aerosol
534 physicochemical properties, *Environ. Sci. Technol.*, 53, 8682-8694, 10.1021/acs.est.9b01019, 2019.
- 535 Seinfeld, J. H. and Pandis, S. N.: *ATMOSPHERIC CHEMISTRY AND PHYSICS: from air pollution to climate*
536 *change*, John Wiley & Sons 2006.
- 537 Shen, C., Zhang, W., Choczynski, J., Davies, J. F., and Zhang, H.: Phase state and relative humidity regulate the
538 heterogeneous oxidation kinetics and pathways of organic-inorganic mixed aerosols, *Environ. Sci. Technol.*,
539 56, 15398-15407, 10.1021/acs.est.2c04670, 2022.
- 540 Srivastava, D., Vu, T. V., Tong, S., Shi, Z., and Harrison, R. M.: Formation of secondary organic aerosols from
541 anthropogenic precursors in laboratory studies, *npj Clim. Atmos. Sci.*, 5, 22, 10.1038/s41612-022-00238-6,
542 2022.
- 543 Wang, C., Lei, Y. D., and Wania, F.: Effect of sodium sulfate, ammonium chloride, ammonium nitrate, and salt
544 mixtures on aqueous phase partitioning of organic compounds, *Environ. Sci. Technol.*, 50, 12742-12749,
545 10.1021/acs.est.6b03525, 2016a.
- 546 Wang, F., Lv, S., Liu, X., Lei, Y., Wu, C., Chen, Y., Zhang, F., and Wang, G.: Investigation into the differences
547 and relationships between gasSOA and aqSOA in winter haze pollution on Chongming Island, Shanghai,
548 based on VOCs observation, *Environ. Pollut.*, 316, 10.1016/j.envpol.2022.120684, 2023.
- 549 Wang, G., Zhang, R., Gomez, M. E., Yang, L., Levy Zamora, M., Hu, M., Lin, Y., Peng, J., Guo, S., Meng, J., Li,



- 550 J., Cheng, C., Hu, T., Ren, Y., Wang, Y., Gao, J., Cao, J., An, Z., Zhou, W., Li, G., Wang, J., Tian, P., Marrero-
551 Ortiz, W., Secretst, J., Du, Z., Zheng, J., Shang, D., Zeng, L., Shao, M., Wang, W., Huang, Y., Wang, Y., Zhu,
552 Y., Li, Y., Hu, J., Pan, B., Cai, L., Cheng, Y., Ji, Y., Zhang, F., Rosenfeld, D., Liss, P. S., Duce, R. A., Kolb,
553 C. E., and Molina, M. J.: Persistent sulfate formation from London Fog to Chinese haze, *Proc. Natl. Acad.*
554 *Sci.*, 113, 13630-13635, 10.1073/pnas.1616540113, 2016b.
- 555 Wang, Y., Cui, S., Fu, X., Zhang, Y., Wang, J., Fu, P., Ge, X., Li, H., and Wang, X.: Secondary organic aerosol
556 formation from photooxidation of C₃H₆ under the presence of NH₃: Effects of seed particles, *Environ. Res.*,
557 211, 10.1016/j.envres.2022.113064, 2022.
- 558 Waxman, E. M., Elm, J., Kurtén, T., Mikkelsen, K. V., Ziemann, P. J., and Volkamer, R.: Glyoxal and
559 methylglyoxal setschenow salting constants in sulfate, nitrate, and chloride solutions: Measurements and
560 gibbs energies, *Environ. Sci. Technol.*, 49, 11500-11508, 10.1021/acs.est.5b02782, 2015.
- 561 Wei, J., Fang, T., and Shiraiwa, M.: Effects of acidity on reactive oxygen species formation from secondary
562 organic aerosols, *ACS Environ. Au*, 2, 336-345, 10.1021/acsenvironau.2c00018, 2022.
- 563 Wong, J. P. S., Lee, A. K. Y., and Abbatt, J. P. D.: Impacts of sulfate seed acidity and water content on isoprene
564 secondary organic aerosol formation, *Environ. Sci. Technol.*, 49, 13215-13221, 10.1021/acs.est.5b02686,
565 2015.
- 566 Yang, L., Huang, R.-J., Yuan, W., Huang, D. D., and Huang, C.: pH-dependent aqueous-phase brown carbon
567 formation: Rate constants and implications for solar absorption and atmospheric photochemistry, *Environ.*
568 *Sci. Technol.*, 58, 1236-1243, 10.1021/acs.est.3c07631, 2024.
- 569 Yaremenko, I. A., Vil', V. A., Demchuk, D. V., and Terent'ev, A. O.: Rearrangements of organic peroxides and
570 related processes, *Beilstein J. Org. Chem*, 12, 1647-1748, 10.3762/bjoc.12.162, 2016.
- 571 You, B., Li, S. Y., Tsona, N. T., Li, J. L., Xu, L., Yang, Z. M., Cheng, S. M., Chen, Q. C., George, C., Ge, M. F.,
572 and Du, L.: Environmental processing of short-chain fatty alcohols induced by photosensitized chemistry
573 of brown carbons, *ACS Earth Space Chem.*, 4, 631-640, 10.1021/acsearthspacechem.0c00023, 2020.
- 574 Zhang, J., Shrivastava, M., Zelenyuk, A., Zaveri, R. A., Surratt, J. D., Riva, M., Bell, D., and Glasius, M.:
575 Observationally constrained modeling of the reactive uptake of isoprene-derived epoxydiols under elevated
576 relative humidity and varying acidity of seed aerosol conditions, *ACS Earth Space Chem.*, 7, 788-799,
577 10.1021/acsearthspacechem.2c00358, 2023.
- 578 Zhang, R., Wang, G., Guo, S., Zamora, M. L., Ying, Q., Lin, Y., Wang, W., Hu, M., and Wang, Y.: Formation of
579 urban fine particulate matter, *Chem. Rev.*, 115, 3803-3855, 10.1021/acs.chemrev.5b00067, 2015a.
- 580 Zhang, S., Li, D., Ge, S., Wu, C., Xu, X., Liu, X., Li, R., Zhang, F., and Wang, G.: Elucidating the mechanism
581 on the transition-metal ion-synergetic-catalyzed oxidation of SO₂ with implications for sulfate formation in
582 Beijing haze, *Environ. Sci. Technol.*, 58, 2912-2921, 10.1021/acs.est.3c08411, 2024.
- 583 Zhang, S., Li, D., Ge, S., Liu, S., Wu, C., Wang, Y., Chen, Y., Lv, S., Wang, F., Meng, J., and Wang, G.: Rapid
584 sulfate formation from synergetic oxidation of SO₂ by O₃ and NO₂ under ammonia-rich conditions:
585 Implications for the explosive growth of atmospheric PM_{2.5} during haze events in China, *Sci. Total Environ.*,
586 772, 144897, 10.1016/j.scitotenv.2020.144897, 2021.
- 587 Zhang, X., Schwantes, R. H., McVay, R. C., Lignell, H., Coggon, M. M., Flagan, R. C., and Seinfeld, J. H.: Vapor
588 wall deposition in Teflon chambers, *Atmos. Chem. Phys.*, 15, 4197-4214, 10.5194/acp-15-4197-2015,
589 2015b.
- 590 Zhao, J., Levitt, N. P., Zhang, R., and Chen, J.: Heterogeneous Reactions of methylglyoxal in acidic media:
591 Implications for secondary organic aerosol formation, *Environ. Sci. Technol.*, 40, 7682-7687,
592 10.1021/es060610k, 2006.
- 593 Zhao, R., Aljawhary, D., Lee, A. K. Y., and Abbatt, J. P. D.: Rapid aqueous-phase photooxidation of dimers in



594 the α -pinene secondary organic aerosol, Environ. Sci. Technol. Lett., 4, 205-210,
595 10.1021/acs.estlett.7b00148, 2017.

596

597

598

599

600

601

602

603



604

605

Figure Captions

606 **Figure 1.** Time evolution of gas-phase and aerosol-phase species in the presence of
607 $(\text{NH}_4)_2\text{SO}_4$ seeds during acetone oxidation process (Phase I: Photooxidation of acetone by
608 OH radicals without NH_3 ; Phase II: Reaction of acetone oxidation products with NH_3 under
609 dark conditions) (a) Gas-phase compounds; (b) SOA and molar ratio of NH_4^+ to SO_4^{2-} in the
610 aerosol-phase; (c) N/C and O/C elemental ratios and oxidation state of compounds (OSc,
611 $2 \times \text{O/C} - \text{H/C}$) of SOA; (d) Relative abundances of CO_2^+ , the sum of CHO^+ plus $\text{C}_2\text{H}_3\text{O}^+$, and
612 CHN family fragments of SOA.

613

614

615

616 **Figure 2.** Fragment compositions of acetone-derived SOA in the presence of $(\text{NH}_4)_2\text{SO}_4$
617 seeds between the two reaction phases. (Phase I: Oxidation of acetone by OH radicals
618 without NH_3 ; Phase II: Reaction of acetone oxidation products with NH_3 under dark
619 conditions)

620

621

622 **Figure 3.** Effect of seed acidity on SOA formation. (a) The amount SOA normalized by the
623 surface area (SA) of aerosols and OSc of SOA in the presence of different seeds at Phase I;
624 (b) Effective Henry's law constants ($K_{\text{H, salt}}$) of MGly and acidity (pH) of inorganic aerosols
625 during the reaction; (c) and (d) Mass spectra of SOA from acetone oxidations by OH
626 radicals with no NH_3 in the presence of Na_2SO_4 and $(\text{NH}_4)_2\text{SO}_4$ seeds, respectively.

627

628

629 **Figure 4.** Effect of ammonia on SOA formation. (a) The Difference in N/C ratio of Phase II
630 relative to Phase I on different seeds; (b) Partitioning coefficients of NH_3 ($\epsilon(\text{NH}_4^+)$) on
631 different seeds in the chamber; (c) MAC of acetone-derived SOA in the presence of different
632 seeds; (d) Mass spectrum of 1H-imidazole-4-carboxylic acid formed during the
633 heterogeneous oxidation of acetone in the presence of $(\text{NH}_4)_2\text{SO}_4$ seed.

634

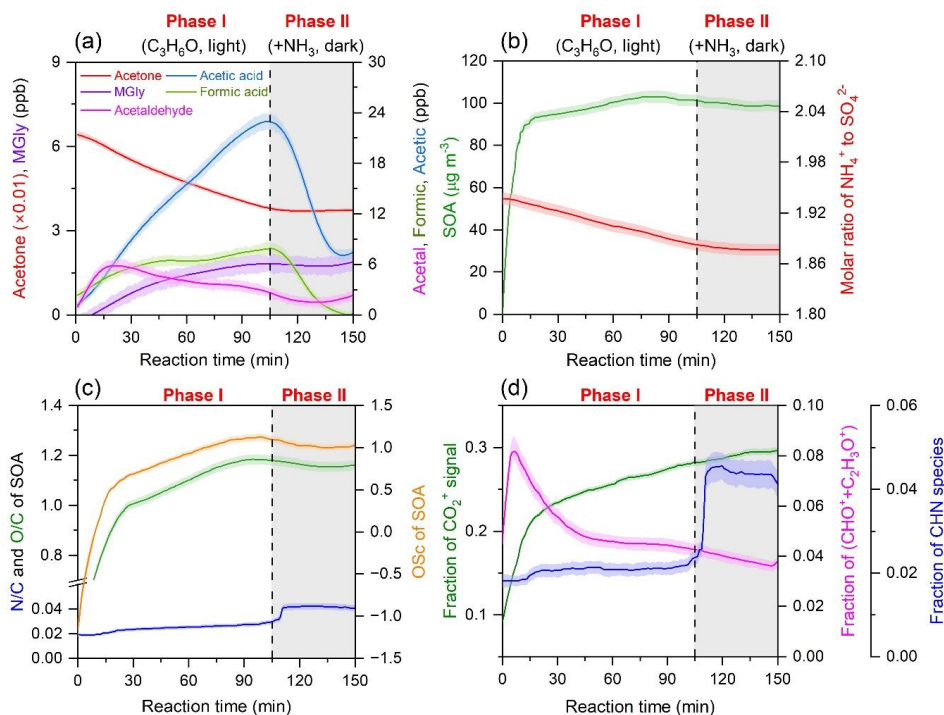
635

636 **Figure 5.** SOA yield (green) and $\text{MAC}_{\lambda=270 \text{ nm}}$ (red) of acetone-derived SOA in the presence
637 of Na_2SO_4 and $(\text{NH}_4)_2\text{SO}_4$ seeds with NH_3 under dark conditions (Phase II), respectively.

638

639 **Figure 6.** A diagram for the formation pathway of SOA derived from acetone oxidation in
640 the atmosphere.

641



642

643 **Figure 1.** Time evolution of gas-phase and aerosol-phase species in the presence of
 644 $(\text{NH}_4)_2\text{SO}_4$ seeds during acetone oxidation process (Phase I: Photooxidation of acetone by
 645 OH radicals without NH_3 ; Phase II: Reaction of acetone oxidation products with NH_3 under
 646 dark conditions) (a) Gas-phase compounds; (b) SOA and molar ratio of NH_4^+ to SO_4^{2-} in the
 647 aerosol-phase; (c) N/C and O/C elemental ratios and oxidation state of compounds (OSc,
 648 $2 \times \text{O}/\text{C} - \text{H}/\text{C}$) of SOA; (d) Relative abundances of CO_2^+ , the sum of CHO^+ plus $\text{C}_2\text{H}_3\text{O}^+$, and
 649 CHN family fragments of SOA.

650

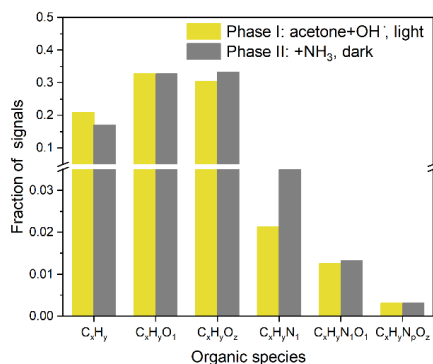
651

652

653

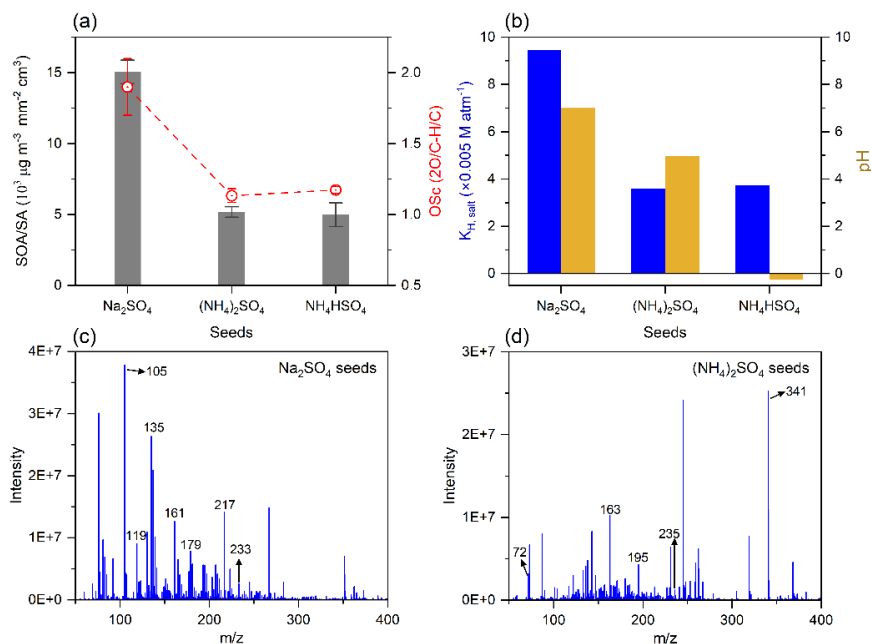
654

655



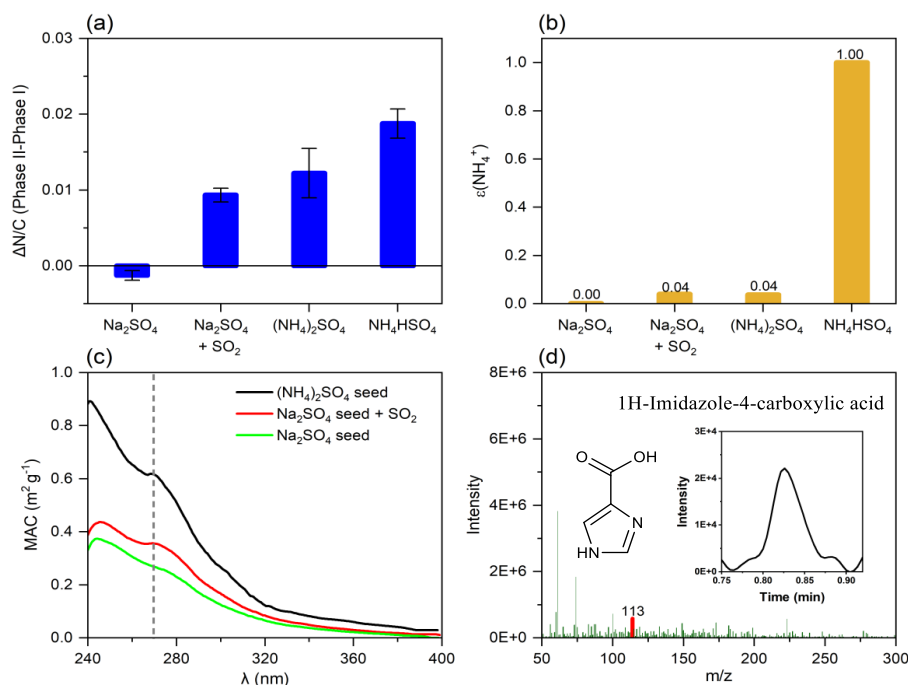
656
657
658
659
660
661
662
663

Figure 2. Fragment compositions of acetone-derived SOA in the presence of (NH₄)₂SO₄ seeds between the two reaction phases. (Phase I: Oxidation of acetone by OH radicals without NH₃; Phase II: Reaction of acetone oxidation products with NH₃ under dark conditions)



664

Figure 3. Effect of seed acidity on SOA formation. (a) The amount SOA normalized by the surface area (SA) of aerosols and OSc of SOA in the presence of different seeds at Phase I; (b) Effective Henry's law constants ($K_{H, \text{salt}}$) of MGly and acidity (pH) of inorganic aerosols during the reaction; (c) and (d) Mass spectra of SOA from acetone oxidations by OH radicals with no NH₃ in the presence of Na₂SO₄ and (NH₄)₂SO₄ seeds, respectively.



670

671 **Figure 4.** Effect of ammonia on SOA formation. (a) The Difference in N/C ratio of Phase II
 672 relative to Phase I on different seeds; (b) Partitioning coefficients of NH₃ ($\epsilon(\text{NH}_4^+)$) on
 673 different seeds in the chamber; (c) MAC of acetone-derived SOA in the presence of different
 674 seeds; (d) Mass spectrum of 1H-imidazole-4-carboxylic acid formed during the
 675 heterogeneous oxidation of acetone in the presence of (NH₄)₂SO₄ seed.

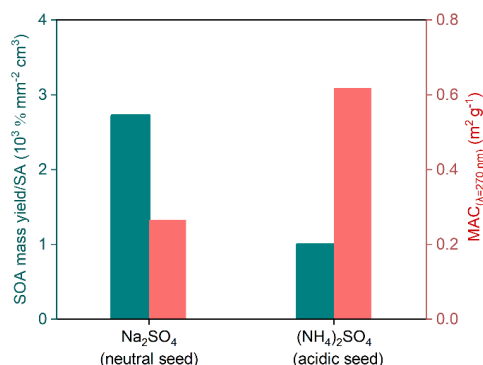
676

677

678

679

680

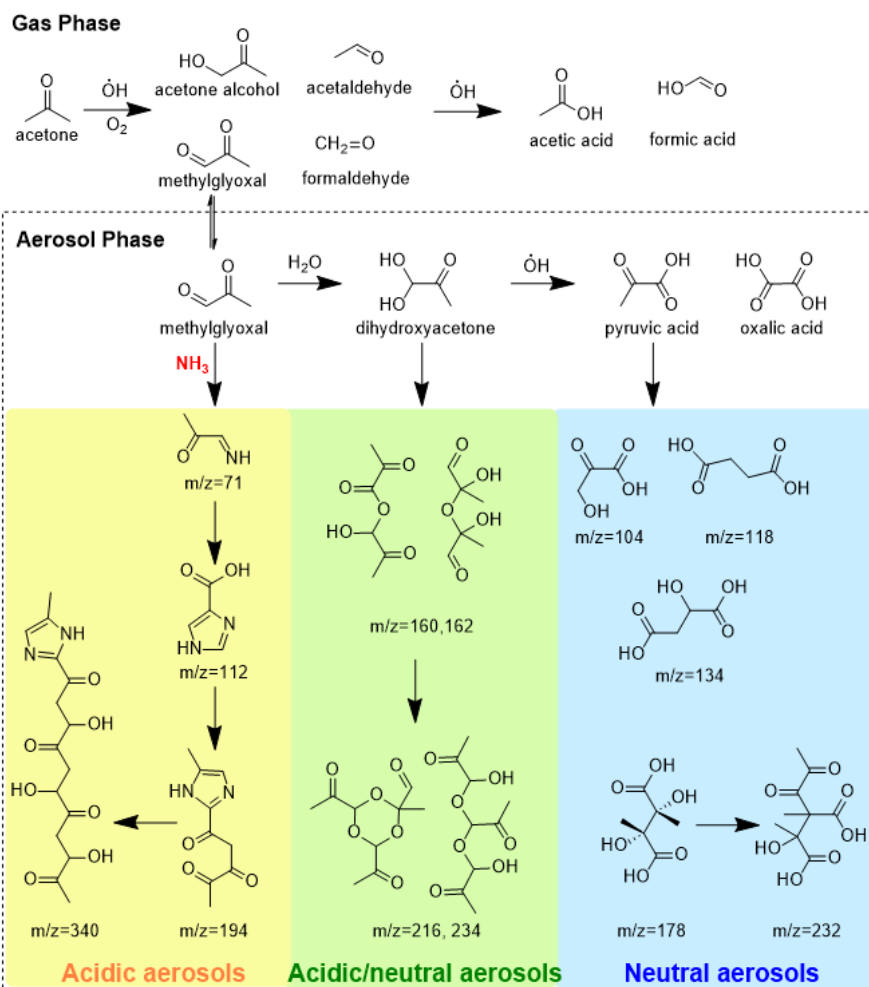


681

682 **Figure 5.** SOA yield (green) and MAC_{λ=270 nm} (red) of acetone-derived SOA in the presence
 683 of Na₂SO₄ and (NH₄)₂SO₄ seeds with NH₃ under dark conditions (Phase II), respectively.



684



685

686 **Figure 6.** A diagram for the formation pathway of SOA derived from acetone oxidation in
 687 the atmosphere.

688